DINAME 2023 - Proceedings of the XIX International Symposium on Dynamic Problems of Mechanics,
A.S. De Paula, A.T. Fabro and M.R. Machado (Editors), ABCM.
Pirenópolis, Go, Brazil, February 26th to March 3rd, 2023

Mechanical Vibration of a Viscoelastic Cantilever Beam with Oscillating Base and Eccentric Tip Mass via Generalized Integral Transform Technique

Gianfranco de M. Stieven[1], **Liviu Nicu**[2], **Renato M. Cotta**[3], **and Carolina P. Naveira-Cotta**[1]

[1] Laboratory of Nano & Microfluidics and Microsystems, LabMEMS, Mechanical Engineering Dept., POLI & COPPE, Universidade Federal do Rio de Janeiro, UFRJ, Brazil

[2] Laboratoire d'Analyse et d'Architecture des Systèmes - LAAS, CNRS, Toulouse, France

[3] General Directorate of Nuclear and Technological Development, Brazilian Navy, Ministry of Defense, RJ, Brazil

Abstract: This work presents an analytical solution to a dynamic model where a homogeneous viscoelastic cantilever beam with an eccentric tip mass is excited by an oscillating base that translates and rotates, and external excitements. The solution is obtained by Generalized Integral Transform Technique (GITT), based on eigenfunctions expansion and an implicit filter. It was verified in forced and free vibration scenarios that internal damping can have an equal or greater influence on the vibratory dynamics of the system than external damping, depending on the geometric and mechanical characteristics of the system. The reduction of vibration irregularities in free vibration from the inclusion of internal damping is also commented on.

Keywords: Analytical Solution, Implicit Filter, Space-State Formulation, Viscoelasticity

INTRODUCTION

A cantilever beam is a horizontal structural element supported at only one end. In vibration problems, this model is used to simplify complex systems and facilitate decision-making. This fact is even more relevant when considering the Euler-Bernoulli beam theory and the inclusion of a tip mass. One of the most prominent applications is in the representation of wind turbines because of its simplicity and ability to effectively represent the wind turbine tower. Abdulraheem and Al-Kindi (2018) studied the dynamic characteristics and structural integrity of wind turbine blades. For that, was considered a mathematical model of a rectangular section cantilever beam with surface crack subjected to harmonic forces, which was validated with experimental data. Rahman et al. (2019) studied how to reduce wind turbine tower vibration using Ant Colony Optimization (ACO) optimized Proportional Integral Derivative (PID) controller. In this study, a cantilever beam represents the wind turbine tower. Adhikari and Bhattacharya (2021) used a cantilever beam model to represent the dynamic response of wind turbines under general harmonic forcing with a damped and flexible foundation. Other applications can be modeled as a cantilever beam, with and without a tip mass. For example, Chen et al (2011) presented an analytical and experimental analysis of the Guangzhou New TV Tower in China, which is a supertall tube-in-tube structure, and the field ambient vibration measurement at different construction stages and under different excitation. Divided into 37 linear elastic beam element segments, the structure was modeled as a cantilever beam. The work of Wahrhaftig, Silva, and Brasil (2019) was concerned with the design improvement of slender structures with reinforced concrete telecommunication towers. This study was based on the assumption of a cantilever beam with lumped masses at the tip of the tower (the antennae and platform). Dehand et al. (2022) presented a clear visualization of how a cantilever beam with a tip mass can represent complex structures such as the wings of an Unmanned Aerial Vehicle (UAV).

Based on their relevance, more sophisticated cantilever beam configurations were considered to represent the physics of even more complex systems. The inclusion of the viscoelastic effect in cantilever beams was one of them. For example, Hijmissen and Van Horssen (2008) considered an Euler-Bernoulli cantilever beam model with tip mass and a Kelvin Voigt viscoelasticity model to determine the deflection in a vertical beam exposed to wind-induced horizontal stresses. However, a more generic cantilever model is rarely seen, containing other physical increments, such as tip mass eccentricity and base rotation. Furthermore, in many cases, the problem of the cantilever beam with or without tip mass is solved numerically, instead of using an analytical solution with low computational cost, favoring the implementation of computationally expensive approaches, such as inverse problems and multi-objective optimization.

Based on that, Matt (2013) developed an analytical solution via the Generalized Integral Transform Technique, for an Euler-Bernoulli cantilever beam problem with an eccentric tip mass, external damping, and an imposed transverse displacement at the clamped end. This method, intensively used approach to fluid and thermal problems such as microscale conjugated heat transfer problems (Silva et al., 2020), transient three-dimensional heat conduction in heterogeneous media (Almeira, Naveira-Cotta, and Cotta, 2020), and supercooled droplets solidification (Carvalho et al., 2021), was based on eigenfunction expansion and on an implicit filter scheme to solve the governing equations for the transverse vibrations.

Matt's contribution in his work is in the analytical solution of the vibratory response of the cantilever beam using

GITT. However, the model presented does not include external influences and internal behavior of the material that, in several applications, would represent an advance in terms of physical enrichment, such as the viscoelasticity of the beam and the rotation of the base. The inclusion of these terms would result in a more complete and more generalized analytical solution to the cantilever beam problem, making it possible to use it for even more complex problems.

Therefore, the main objective of this work is to present an improvement of the dynamic problem considered by Matt (2013), proposing an analytical solution to a cantilever beam modeled by Euler Bernoulli's theory taking into account: (1) a viscoelastic beam using the Kelvin-Voigt model; (2) external damping; (3) eccentric tip mass and; (4) an oscillating base that translates and rotates. The solution of this system will be carried out via the Generalized Integral Transform Technique, from the implementation of an implicit filter and by eigenfunctions expansion (Matt, 2013).

It is important to emphasize that, according to the authors' knowledge, the inclusion of this viscoelastic mechanical behavior in an exact analytical solution by the Generalized Integral Transform Technique is new in the literature and can be quite useful as a benchmark solution for inverse applications of lifting the uncertainty of mechanical properties and even in the construction of simulation-based artificial intelligence.

DISTRIBUTED PARAMETER FORMULATION

For this problem, consider a viscoelastic cantilever beam made of homogeneous material, supported by an oscillating base at $x = 0$, and with an eccentric tip mass at $x = L$ as shown on Fig. 1. The mathematical representation can be described on Eq. 1 to 5,

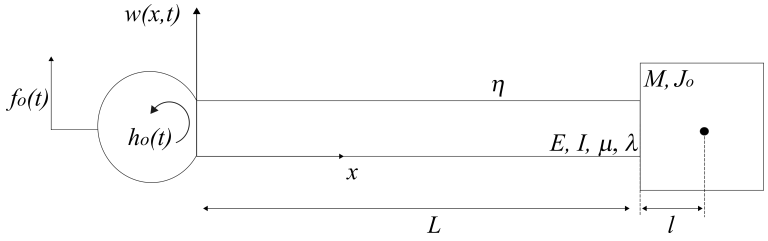

Figure 1 – Schematic representation of a homogeneous cantilever beam with an oscillating base and eccentric tip mass.

$$EIw''''(x,t) + \mu\ddot{w}(x,t) + \eta\dot{w}(x,t) + \lambda\dot{w}''''(x,t) = f(x,t) \tag{1}$$

considering the boundary conditions,

$$w(0,t) = f_0(t) \tag{2}$$

$$w'(0,t) = h_0(t) \tag{3}$$

$$EIw''(L,t) = -\left(J_0 + Ml^2\right)\ddot{w}'(L,t) - Ml\ddot{w}(L,t) - \lambda\dot{w}''(L,t) \tag{4}$$

$$EIw'''(L,t) = M\ddot{w}(L,t) + Ml\ddot{w}'(L,t) - \lambda\dot{w}'''(L,t) \tag{5}$$

and initial conditions: $w(x,0) = w_0(x)$ and $\dot{w}(x,0) = v_0(x)$ which represent the initial displacement and velocity of the beam, respectively. In these equations, $w(x,t)$ represents the beam deflection [m], E the beam Young's modulus [Pa], I the beam area moment of inertia [m^4], μ the beam mass distribution [kg m^{-1}], η and λ, respectively, the external [N s m^{-2}] and internal [N s m^2] damping coefficient, $f(x,t)$ the density per unit length of applied vertical forces [N m^{-1}], $f_0(t)$ and $h_0(t)$, respectively, the base translation and rotation, M, J_0 and l, respectively, the tip mass magnitude at $x = L$ [kg], the tip mass moment of inertia [kg m^2] and the distance between the tip mass center of gravity and its attachment point at the end of the cantilever beam [m].

Dimensionless Formulation

For dimensionless variables it is considered $X \equiv x/L$, $\tau = \Omega t$, and $W(X,\tau) \equiv w(x,t)/D$, where Ω and D represent, respectively, a characteristic frequency and dimension of the cross section of the system. Applying the dimensionless variables, presented above, in Eq. 1, one obtains,

$$W''''(X,\tau) + \mu^*\ddot{W}(X,\tau) + \eta^*\dot{W}(X,\tau) + \lambda^*\dot{W}''''(X,\tau) = F(X,\tau) \tag{6}$$

where $F(X,\tau) = \frac{L^4}{EI\,D} f(XL, \tau/\Omega)$ is the dimensionless external exciting force, and $\mu^* = \mu\Omega^2L^4/EI$, $\eta^* = \eta\Omega L^4/EI$, and $\lambda^* = \lambda\Omega/EI$. Deriving the dimensionless the boundary conditions versions, one can have,

$$W(0,\tau) = \frac{1}{D} f_0(\tau/\Omega) = F_0(\tau) \tag{7}$$

$$W'(0,\tau) = \frac{L}{D} h_0(\tau/\Omega) = H_0(\tau) \tag{8}$$

$$W''(1,\tau) = -\left(\beta + \alpha\varepsilon^2\right)\mu^* \ddot{W}'(1,\tau) - \alpha\varepsilon\mu^* \ddot{W}(1,\tau) - \lambda^* \dot{W}''(1,\tau) \tag{9}$$

$$W'''(1,\tau) = \alpha\mu^* \ddot{W}(1,\tau) + \alpha\varepsilon\mu^* \ddot{W}'(1,\tau) - \lambda^* \dot{W}'''(1,\tau) \tag{10}$$

and initial conditions, $W(X,0) = w_0(XL)/D \equiv W_0(X)$ and $\dot{W}(X,0) = v_0(XL)/\Omega D \equiv V_0(X)$, where $\alpha = M/\mu L$, $\beta = J_0/\mu L^3$, and $\varepsilon = l/L$. Here, Ω is chosen as the first natural frequency of the cantilever beam without the tip mass (Matt (2013)).

INTEGRAL TRANSFORM APPLYING AN IMPLICIT FILTER SCHEME

In this method, the first step is to split the solution into two by applying this implicit filter scheme (Matt, 2013),

$$W(X,\tau) = \phi(X,\tau) + W_F(X;\tau) \tag{11}$$

where $\phi(X,\tau)$ is an unknown potential, and; $W_F(X;\tau)$ is a filter carefully selected in order to consider all non-homogeneous boundary conditions in a simplified way. It was chosen $W_F''''(X;\tau) = 0$. Using Eq. 11 in Eq. 7 and 8, and to provide homogeneous boundary conditions for ϕ, $\phi(0,\tau) = \phi'(0,\tau) = 0$, and $W_F(X;\tau) = F_0(\tau) + H_0(\tau)X + C_2(\tau)X^2 + C_3(\tau)X^3$. Substituting Eq. 11 and the expression of $W_F(X;\tau)$ in Eq. 6, it results in,

$$\begin{aligned}\phi''''(X,\tau) + \mu^*\ddot{\phi}(X,\tau) + \eta^*\dot{\phi}(X,\tau) + \lambda^*\dot{\phi}''''(X,\tau) + \mu^* X^2 \ddot{C}_2(\tau) + \mu^* X^3 \ddot{C}_3(\tau) + \eta^* X^2 \dot{C}_2(\tau) + \eta^* X^3 \dot{C}_3(\tau) \\ = F(X,\tau) - \mu^* \ddot{F}_0(\tau) - \mu^* X \ddot{H}_0(\tau) - \eta^* \dot{F}_0(\tau) - \eta^* X \dot{H}_0(\tau) = \tilde{F}(X,\tau)\end{aligned} \tag{12}$$

where $\tilde{F}(X,\tau)$ represents a modified external excitation. Inserting $W(X,\tau) = \phi(X,\tau) + W_F(X;\tau)$ in the first boundary condition in $X = 1$ given by Eq. 9, and for homogeneous boundary condition, $\phi''(1,\tau) = 0$, one obtains Eq. 13. Repeating the above procedure for the second boundary condition on $X = 1$, for the same purpose presented above, $\phi'''(1,\tau) = 0$, one has Eq. 14.

$$\begin{aligned}&\ddot{C}_2(\tau)\left[2\mu^*\left(\beta + \alpha\varepsilon^2\right) + \alpha\varepsilon\mu^*\right] + \ddot{C}_3(\tau)\left[3\mu^*\left(\beta + \alpha\varepsilon^2\right) + \alpha\varepsilon\mu^*\right] + 2\lambda^*\dot{C}_2(\tau) + 6\lambda^*\dot{C}_3(\tau) + 2C_2(\tau) \\ &+6C_3(\tau) + \mu^*\left(\beta + \alpha\varepsilon^2\right)\ddot{\phi}'(1,\tau) + \alpha\varepsilon\mu^*\ddot{\phi}(1,\tau) = -\alpha\varepsilon\mu^*\ddot{F}_0(\tau) - \mu^*\left(\beta + \alpha\varepsilon^2\right)\ddot{H}_0(\tau) - \alpha\varepsilon\mu^*\ddot{H}_0(\tau)\end{aligned} \tag{13}$$

$$\begin{aligned}\ddot{C}_2(\tau)\left[2\alpha\varepsilon\mu^* + \alpha\mu^*\right] + \ddot{C}_3(\tau)\left[3\alpha\varepsilon\mu^* + \alpha\mu^*\right] - 6\lambda^*\dot{C}_3(\tau) - 6C_3(\tau) + \alpha\mu^*\ddot{\phi}(1,\tau) + \alpha\varepsilon\mu^*\ddot{\phi}'(1,\tau) = \\ -\alpha\mu^*\ddot{F}_0(\tau) - \alpha\mu^*\ddot{H}_0(\tau) - \alpha\varepsilon\mu^*\ddot{H}_0(\tau)\end{aligned} \tag{14}$$

Substituting $W(X,\tau) = \phi(X,\tau) + W_F(X;\tau)$ in the initial condition of $W(X,\tau)$, one can see that: supposing $C_2(0) = C_3(0) = 0$, it results in $\phi(X,0) = W_0(X)$ - $F_0(0)$ - $H_0(0)X$ and; supposing $\dot{C}_2(0) = \dot{C}_3(0) = 0$, it results in $\dot{\phi}(X,0) = V_0(X) - \dot{F}_0(0) - \dot{H}_0(0)X$.

Eigenfunction Expansion

The integral transform solution requires the performance of three tasks. The first task is to define the inverse-transform pair of this problem. It is defined:

$$\bar{\phi}_m(\tau) = \int_0^1 \tilde{\Psi}_m(X)\phi(X,\tau)dX \qquad Transform \tag{15}$$

$$\phi(X,\tau) = \sum_{m=1}^{\infty} \tilde{\Psi}_m(X)\bar{\phi}_m(\tau) \qquad Inverse \tag{16}$$

The second task is to define an auxiliary boundary eigenvalue problem in order to generate the eigenvalues and eigenfunctions for the series expansion of the unknown potential $\phi(X,\tau)$. The auxiliary boundary eigenvalue problem chosen was:

$$\Psi_m''''(X) - \zeta_m^4 \Psi_m(X) = 0 \tag{17}$$

with boundary conditions,

$$\Psi_m(0) = \Psi_m'(0) = \Psi_m''(1) = \Psi_m'''(1) = 0 \tag{18}$$

The boundary eigenvalue problem defined by Eq. 17 and 18 has the following analytical solution,

$$\Psi_m(X) = \sin(\zeta_m X) - \sinh(\zeta_m X) - \left(\sin(\zeta_m) + \sinh(\zeta_m)\right)\left[\cos(\zeta_m X) - \cosh(\zeta_m X)\right]/\cos(\zeta_m) + \cosh(\zeta_m) \tag{19}$$

considering the transcendental equation $\cos(\zeta_m)\cosh(\zeta_m) = -1$. It is verifiable that,

$$\int_0^1 \Psi_m(X)\Psi_n(X)dX = N_\Psi(\zeta_m)\delta_{m,n}, \quad \delta_{m,n} = 0,\ if\ m \neq n\ or\ 1,\ if\ m = n \tag{20}$$

where $N_\Psi(\zeta_m)$ stands for the normalization integral obtained based on the orthogonality property. It is convenient to consider $\tilde{\Psi}_m(X) = \Psi_m(X)/N_\Psi(\zeta_m)^{1/2}$. The third and final task of this step is to perform the integral transform in Eq. 12 operating on it with $\int_0^1(.)\tilde{\Psi}_m(X)dX$, in addition to replacing the relationship expressed in Eq. 16 in Eq. 13 and 14, in the sense of expressing the spatial and temporal derivatives of $\phi(X,\tau)$ in $X=1$ in terms of the transformed potential $\bar{\phi}_m(\tau)$. The ODE below is obtained,

$$\begin{aligned}&\ddot{\bar{\phi}}_m(\tau)+\left[\zeta_m^4\lambda^*/\mu^*+\eta^*/\mu^*\right]\dot{\bar{\phi}}_m(\tau)+\zeta_m^4/\mu^*\bar{\phi}_m(\tau) \\ &+A_m\ddot{C}_2(\tau)+B_m\ddot{C}_3(\tau)+\eta^*/\mu^*A_m\dot{C}_2(\tau)+\eta^*/\mu^*B_m\dot{C}_3(\tau)=1/\mu^*\bar{\bar{F}}_m(\tau)\end{aligned} \tag{21}$$

where $A_m=\int_0^1 X^2\tilde{\Psi}_m(X)dX$, $B_m=\int_0^1 X^3\tilde{\Psi}_m(X)dX$, and $\bar{\bar{F}}_m(\tau)=\int_0^1\tilde{F}(X,\tau)\tilde{\Psi}_m(X)dX$. Substituting the inverse relationship given by Eq. 16 in Eqs. 13 and 14, these two ODEs are obtained:

$$\begin{aligned}&\left[2\mu^*\left(\beta+\alpha\varepsilon^2\right)+\alpha\varepsilon\mu^*\right]\ddot{C}_2(\tau)+\left[3\mu^*\left(\beta+\alpha\varepsilon^2\right)+\alpha\varepsilon\mu^*\right]\ddot{C}_3(\tau)+2\lambda^*\dot{C}_2(\tau)+6\lambda^*\dot{C}_3(\tau)+2C_2(\tau)+6C_3(\tau) \\ &+\mu^*\left(\beta+\alpha\varepsilon^2\right)\sum_{m=1}^{\infty}\tilde{\Psi}'_m(1)\ddot{\bar{\phi}}_m(\tau)+\alpha\varepsilon\mu^*\sum_{m=1}^{\infty}\tilde{\Psi}_m(1)\ddot{\bar{\phi}}_m(\tau)=-\alpha\varepsilon\mu^*\ddot{F}_0(\tau)-\left\{\mu^*\left[\beta+\alpha\varepsilon\left(\varepsilon+1\right)\right]\right\}\ddot{H}_0(\tau)\end{aligned} \tag{22}$$

$$\begin{aligned}&\left[2\alpha\varepsilon\mu^*+\alpha\mu^*\right]\ddot{C}_2(\tau)+\left[3\alpha\varepsilon\mu^*+\alpha\mu^*\right]\ddot{C}_3(\tau)-6\lambda^*\dot{C}_3(\tau)-6C_3(\tau)+\alpha\mu^*\sum_{m=1}^{\infty}\tilde{\Psi}_m(1)\ddot{\bar{\phi}}_m(\tau) \\ &+\alpha\varepsilon\mu^*\sum_{m=1}^{\infty}\tilde{\Psi}'_m(1)\ddot{\bar{\phi}}_m(\tau)=-\alpha\mu^*\ddot{F}_0(\tau)-\left[\alpha\mu^*\left(1+\varepsilon\right)\right]\ddot{H}_0(\tau)\end{aligned} \tag{23}$$

Equations 21, 22 and 23 must be solved simultaneously. The coupled system of ODEs presented in Eqs. 21, 22 and 23 is subject to initial conditions $C_2(0)=C_3(0)=\dot{C}_2(0)=\dot{C}_3(0)=0$, $\bar{\phi}_m(0)=\bar{\phi}_{0,m}$ and $\dot{\bar{\phi}}_m(0)=\dot{\bar{\phi}}_{0,m}$, such that $\bar{\phi}_{0,m}=\int_0^1\tilde{\Psi}_m(X)\left[W_0(X)-F_0(0)-H_0(0)X\right]dX$, and $\dot{\bar{\phi}}_{0,m}=\int_0^1\tilde{\Psi}_m(X)\left[V_0(X)-\dot{F}_0(0)-\dot{H}_0(0)X\right]dX$.

ANALYTICAL SOLUTION VIA MATRIX EIGENSYSTEM ANALYSIS

The differential system given by Eqs. 21, 22 and 23 can be rewritten as a system of ordinary first-order differential equations using a state-space formulation. By definition the state vector $\mathbf{z}(\tau)$ is such that,

$$\mathbf{z}(\tau)=\left[\bar{\phi}_1(\tau)\cdots\bar{\phi}_{N_T}(\tau),C_2(\tau),C_3(\tau),\dot{\bar{\phi}}_1(\tau)\cdots\dot{\bar{\phi}}_{N_T}(\tau),\dot{C}_2(\tau),\dot{C}_3(\tau)\right]^{\mathrm{T}} \tag{24}$$

where one can rewrite Eqs. 21, 22 and 23 in a matrix form as,

$$\mathbf{A}\dot{\mathbf{z}}(\tau)=\mathbf{B}\mathbf{z}(\tau)+\mathbf{C}(\tau) \tag{25}$$

where the components of the constant matrices $\mathbf{A}$ and $\mathbf{B}$, $A_{p,q}$ and $B_{p,q}$, and the source vector $\mathbf{C}(\tau)$, $C_p(\tau)$, $p,q=1,2,\cdots,2N_T+4$. Premultiplying Eq. 25 for $\mathbf{A}^{-1}$ the system of equations can be written as,

$$\dot{\mathbf{z}}(\tau)=\Lambda\mathbf{z}(\tau)+\mathbf{L}(\tau) \tag{26}$$

where $\Lambda=\mathbf{A}^{-1}\mathbf{B}$ and $\mathbf{L}(\tau)=\mathbf{A}^{-1}\mathbf{C}(\tau)$. Defining $\mathbf{z}(\tau)=\Xi_R\xi(\tau)$ and substituting in Eq. 26, one can obtain,

$$\Xi_R\dot{\xi}(\tau) = \Lambda\Xi_R\xi(\tau)+\mathbf{L}(\tau) \tag{27}$$

$$\xi(0) = \xi_0 \tag{28}$$

The Ξ_R corresponds to the matrix whose columns are the right eigenvectors of Λ. Considering $\Xi_L^T\Xi_R=\mathbf{I}$, one obtains:

$$\dot{\xi}(\tau)=\Lambda_\xi\xi(\tau)+\mathbf{L}_\xi(\tau) \tag{29}$$

The solution of Eq. 27 is a decoupled system of first-order linear ordinary differential equations, that can be expressed as,

$$\xi_j(\tau)=\xi_{0,j}\,e^{\lambda_j\tau}+\int_0^\tau e^{\lambda_j(\tau-\tau^*)}L_{\xi,j}(\tau^*)d\tau^* \tag{30}$$

that is:

$$z_m(\tau)=\sum_{j=1}^{2N_T+4}\Xi_{R_{m,j}}\xi_j(\tau),\qquad m=1,2,...,2N_T+4 \tag{31}$$

The exact dimensionless solution given by Eqs. from 6 to 10, can be directly computed with the expressions: $\phi(X,\tau)=\sum_{m=1}^{N_T}\tilde{\Psi}_m(X)z_m(\tau)$, $W_F(X;\tau)=F_0(\tau)+XH_0(\tau)+X^2z_{N_T+1}(\tau)+X^3z_{N_T+2}(\tau)$ and $W(X,\tau)=\phi(X,\tau)+W_F(X;\tau)$.

One can visually check the matrices $\mathbf{A}$, $\mathbf{B}$ and $\mathbf{C}(\tau)$ considering $N_T=1$ such as,

$$\begin{bmatrix}1&0&0&0&0&0\\0&1&0&0&0&0\\0&0&1&0&0&0\\0&0&0&1&A_1&B_1\\0&0&0&a_1&\chi_1&\chi_2\\0&0&0&b_1&\chi_3&\chi_4\end{bmatrix}\begin{bmatrix}\dot{\bar{\phi}}_1(\tau)\\\dot{C}_2(\tau)\\\dot{C}_3(\tau)\\\ddot{\bar{\phi}}_1(\tau)\\\ddot{C}_2(\tau)\\\ddot{C}_3(\tau)\end{bmatrix}=\begin{bmatrix}0&0&0&1&0&0\\0&0&0&0&1&0\\0&0&0&0&0&1\\\hat{\zeta}_1&0&0&\hat{\zeta}_{\lambda 1}&\hat{\eta}A_1&\hat{\eta}B_1\\0&-2&-6&0&-2\lambda^*&-6\lambda^*\\0&0&6&0&0&6\lambda^*\end{bmatrix}\begin{bmatrix}\bar{\phi}_1(\tau)\\C_2(\tau)\\C_3(\tau)\\\dot{\bar{\phi}}_1(\tau)\\\dot{C}_2(\tau)\\\dot{C}_3(\tau)\end{bmatrix}+\begin{bmatrix}0\\0\\0\\\frac{1}{\mu^*}\bar{\bar{F}}_1(\tau)\\\hat{F}_1(\tau)\\\hat{F}_2(\tau)\end{bmatrix} \tag{32}$$

where the constants, for $m = 1, 2, \cdots, N_T$, are given by,

$$a_m = \mu^* \left(\beta + \alpha\varepsilon^2\right) \frac{\mathrm{d}\tilde{\Psi}_m(1)}{\mathrm{d}X} + \alpha\varepsilon\mu^* \tilde{\Psi}_m(1) \tag{33}$$

$$b_m = \alpha\varepsilon\mu^* \frac{\mathrm{d}\tilde{\Psi}_m(1)}{\mathrm{d}X} + \alpha\mu^* \tilde{\Psi}_m(1) \tag{34}$$

$$\chi_1 = 2\mu^* \left(\beta + \alpha\varepsilon^2\right) + \alpha\varepsilon\mu^* \tag{35}$$

$$\chi_2 = 3\mu^* \left(\beta + \alpha\varepsilon^2\right) + \alpha\varepsilon\mu^* \tag{36}$$

$$\chi_3 = 2\alpha\varepsilon\mu^* + \alpha\mu^* \tag{37}$$

$$\chi_4 = 3\alpha\varepsilon\mu^* + \alpha\mu^* \tag{38}$$

$$\hat{F}_1(\tau) = -\alpha\varepsilon\mu^* \frac{\mathrm{d}^2 F_0(\tau)}{\mathrm{d}\tau^2} - \left\{\mu^* \left[\beta + \alpha\varepsilon\left(\varepsilon + 1\right)\right]\right\} \frac{\mathrm{d}^2 H_0(\tau)}{\mathrm{d}\tau^2} \tag{39}$$

$$\hat{F}_2(\tau) = -\alpha\mu^* \frac{\mathrm{d}^2 F_0(\tau)}{\mathrm{d}\tau^2} - \left[\alpha\mu^* \left(1 + \varepsilon\right)\right] \frac{\mathrm{d}^2 H_0(\tau)}{\mathrm{d}\tau^2} \tag{40}$$

where $\hat{\zeta}_1 = -\frac{\zeta_1^4}{\mu^*}$, $\hat{\eta} = -\frac{\eta^*}{\mu^*}$, and $\hat{\zeta}_{\lambda\,1} = \hat{\eta} + \hat{\zeta}_1 \lambda^*$. Expanding these terms to $N_T \geq 1$, one can obtain,

$$[\mathbf{A}] = A_{p,q} = \begin{cases} \delta_{p,q} & \text{for } 1 \leq p,q \leq 2N_T + 2 \\ a_{q-(N_T+2)} & \text{for } p = 2N_T + 3, N_T + 2 < q \leq 2N_T + 2 \\ b_{q-(N_T+2)} & \text{for } p = 2N_T + 4, N_T + 2 < q \leq 2N_T + 2 \\ A_{p-(N_T+2)} & \text{for } q = 2N_T + 3, N_T + 2 < p \leq 2N_T + 2 \\ B_{p-(N_T+2)} & \text{for } q = 2N_T + 4, N_T + 2 < p \leq 2N_T + 2 \\ \chi_1 & \text{for } p = 2N_T + 3, q = 2N_T + 3 \\ \chi_2 & \text{for } p = 2N_T + 3, q = 2N_T + 4 \\ \chi_3 & \text{for } p = 2N_T + 4, q = 2N_T + 3 \\ \chi_4 & \text{for } p = 2N_T + 4, q = 2N_T + 4 \\ 0 & \text{otherwise} \end{cases} \tag{41}$$

$$[\mathbf{B}] = B_{p,q} = \begin{cases} \delta_{p,q-(N_T+2)} & \text{for } 1 \leq p \leq N_T + 2, N_T + 2 < q \leq 2N_T + 4 \\ -\frac{1}{\mu^*} \zeta_{p-(N_T+2)}^4 & \text{for } N_T + 2 < p \leq 2N_T + 2, 1 \leq q \leq N_T \\ -\frac{1}{\mu^*} \left(\zeta_{p-(N_T+2)}^4 \lambda^* + \eta^*\right) & \text{for } N_T + 2 < p \leq 2N_T + 2, N_T + 2 < q \leq 2N_T + 2 \\ -\frac{\eta^*}{\mu^*} A_{p-(N_T+2)} & \text{for } N_T + 2 < p \leq 2N_T + 2, q = 2N_T + 3 \\ -\frac{\eta^*}{\mu^*} B_{p-(N_T+2)} & \text{for } N_T + 2 < p \leq 2N_T + 2, q = 2N_T + 4 \\ -2 & \text{for } p = 2N_T + 3, q = N_T + 1 \\ -6 & \text{for } p = 2N_T + 3, q = N_T + 2 \\ 6 & \text{for } p = 2N_T + 4, q = N_T + 2 \\ -2\lambda^* & \text{for } p = 2N_T + 3, q = 2N_T + 3 \\ -6\lambda^* & \text{for } p = 2N_T + 3, q = 2N_T + 4 \\ 6\lambda^* & \text{for } p = 2N_T + 4, q = 2N_T + 4 \\ 0 & \text{otherwise} \end{cases} \tag{42}$$

$$[\mathbf{C}] = C_p(\tau) = \begin{cases} 0 & \text{for } 1 \leq p \leq N_T + 2 \\ \frac{1}{\mu^*} \bar{\bar{F}}_{p-(N_T+2)}(\tau) & \text{for } N_T + 2 < p \leq 2N_T + 2 \\ \hat{F}_1(\tau) & \text{for } p = 2N_T + 3 \\ \hat{F}_2(\tau) & \text{for } p = 2N_T + 4 \end{cases} \tag{43}$$

where $\delta_{p,q}$ represents the Kronecker delta tensor.

COMPUTATIONAL VERIFICATION

In this section, the computational verification of the presented model will be carried out considering numerical results of Matt (2013). The solution proposed in this paper was numerically implemented using FORTRAN in the Microsoft Visual Studio 2019 computing environment. All comparisons in this section will not consider initial displacement, internal dampings, external vertical forces and rotation. For this section, consider an aluminum cantilever beam with Young's modulus E = 69 GPa and specific mass ρ = 2700 kg m^{-3}. The length of the beam is L = 1 m and it has a circular section

with diameter D = 10 mm. The mass per unit length is μ = 0.212 kg m^{-1} and the first circular natural frequency without a tip mass is Ω = 44.442 rad s^{-1}. So μ^* = 12.362. First, consider a free vibration case consider a free vibration for a damped beam with properties values presented on Tab. 1, which results are expressed in Tab. 2. Results are shown

Table 1 – Parameter values for free and forced vibration analysis.

System/Parameter	α	β	ε	η	λ	$F_0(\tau)$	$H_0(\tau)$	$W_0(X)$	$V_0(X)$
Free Vibration	10	0.5	0.1	0.05	0	0	0	0	$0.225\sin(\pi X)$
Forced Vibration	10	0.5	0.1	0.05	0	$0.5\sin(\nu\tau)$	0	0	0

for four different values of X, $X \in [0.25, 0.50, 0.75, 1.00]$, for three different dimensionless times τ, $\tau \in [1, 10, 100]$ and for four (increasing) values of N_T, $N_T \in [5, 10, 20, 30]$. For this computational verification, α, β and ε are respectively 10, 0.5 and 0.1. Observing the results, in most cases it is possible to obtain a solution with at least five decimal places considering N_T from 5 to 30, for all temporal and spatial values. In terms of accuracy, for this case, $N_T = 20$ is quite acceptable for converged values, in all cases. For the second set of data to be verified, that is, a forced vibration system,

Table 2 – Displacement convergence considering free vibration.

	$\alpha = 10$, $\beta = 0.5$ e $\varepsilon = 0.1$ (Matt (2013))				$\alpha = 10$, $\beta = 0.5$ e $\varepsilon = 0.1$ (Present Work)			
	$N_T = 5$	$N_T = 10$	$N_T = 20$	$N_T = 30$	$N_T = 5$	$N_T = 10$	$N_T = 20$	$N_T = 30$
$\tau = 1$								
$X = 0.25$	0.028671	0.032790	0.032308	0.032308	0.028669	0.032789	0.032326	0.032325
$X = 0.50$	0.077120	0.087834	0.086519	0.086519	0.077114	0.087830	0.086567	0.086568
$X = 0.75$	0.083764	0.093223	0.091902	0.091902	0.083758	0.093219	0.091950	0.091950
$X = 1.00$	$3.79458.10^{-4}$	$-1.0310.10^{-2}$	$-9.54159.10^{-3}$	$-9.54159.10^{-3}$	$3.78334.10^{-4}$	$-1.03119.10^{-2}$	$-9.57720.10^{-3}$	$-9.57720.10^{-3}$
$\tau = 10$								
$X = 0.25$	-0.031707	-0.047753	-0.046262	-0.046262	-0.031704	-0.047750	-0.046322	-0.046322
$X = 0.50$	-0.137958	-0.194781	-0.189321	-0.189321	-0.137935	-0.194770	-0.189538	-0.189538
$X = 0.75$	-0.312768	-0.429200	-0.418233	-0.418233	-0.312744	-0.429182	-0.418677	-0.418677
$X = 1.00$	-0.523057	-0.710986	-0.693246	-0.693246	-0.523024	-0.710965	-0.693969	-0.693969
$\tau = 100$								
$X = 0.25$	-0.035601	-0.043677	-0.043114	-0.043114	-0.035619	-0.043704	-0.043166	-0.043166
$X = 0.50$	-0.103442	-0.127197	-0.124868	-0.124868	-0.103475	-0.127230	-0.124994	-0.124994
$X = 0.75$	-0.156813	-0.198257	-0.194135	-0.194135	-0.156835	-0.198283	-0.194332	-0.194332
$X = 1.00$	-0.172279	-0.228838	-0.223372	-0.223372	-0.172267	-0.228828	-0.223592	-0.223592

the parameter values are also presented on Tab. 1 and results are expressed in Tab. 3. The parameter $\nu = 0.128191$ is the first dimensionless damped natural frequency for the chosen values of α, β, ε and η. For this comparison, consider the truncation order N_T such that $N_T \in [20, 30, 40, 50]$, the same values of X, $X \in [0.25, 0.50, 0.75, 1.00]$, and three different dimensionless times τ, $\tau \in [0.01, 25, 50]$. The results shown in Tab. 3 expose convergence and numerical stability of the

Table 3 – Displacement convergence of forced vibration.

	$\alpha = 10$, $\beta = 0.5$ e $\varepsilon = 0.1$ (Matt, 2013)				$\alpha = 10$, $\beta = 0.5$ e $\varepsilon = 0.1$ (Present Work)			
	$N_T = 20$	$N_T = 30$	$N_T = 40$	$N_T = 50$	$N_T = 20$	$N_T = 30$	$N_T = 40$	$N_T = 50$
$\tau = 0.01$								
$X = 0.25$	$3.0622.10^{-5}$	$3.1964.10^{-5}$	$3.2326.10^{-5}$	$3.2385.10^{-5}$	$3.0645.10^{-5}$	$3.1987.10^{-5}$	$3.2343.10^{-5}$	$3.2470.10^{-5}$
$X = 0.50$	$-1.7781.10^{-6}$	$-2.1683.10^{-6}$	$-2.1683.10^{-6}$	$-2.1683.10^{-6}$	$-1.8195.10^{-6}$	$-2.1911.10^{-6}$	$-2.1911.10^{-6}$	$-2.1911.10^{-6}$
$X = 0.75$	$2.0960.10^{-6}$	$2.0960.10^{-6}$	$2.0960.10^{-6}$	$2.0960.10^{-6}$	$1.9591.10^{-6}$	$1.9591.10^{-6}$	$1.9591.10^{-6}$	$1.9591.10^{-6}$
$X = 1.00$	$3.3251.10^{-5}$	$3.3251.10^{-5}$	$3.3251.10^{-5}$	$3.3251.10^{-5}$	$3.3577.10^{-5}$	$3.3578.10^{-5}$	$3.3578.10^{-5}$	$3.3578.10^{-5}$
$\tau = 25$								
$X = 0.25$	0.032345	0.032346	0.032346	0.032347	0.032427	0.032427	0.032428	0.032428
$X = 0.50$	0.198871	0.198873	0.198873	0.198873	0.199116	0.199118	0.199118	0.199118
$X = 0.75$	0.415951	0.415951	0.415951	0.415951	0.416280	0.416280	0.416280	0.416280
$X = 1.00$	0.639891	0.639891	0.639891	0.639891	0.639988	0.639988	0.639988	0.639988
$\tau = 50$								
$X = 0.25$	-0.043105	-0.043105	-0.043105	-0.043104	-0.043143	-0.043141	-0.043142	-0.043142
$X = 0.50$	-0.326851	-0.326849	-0.326849	-0.326849	-0.326872	-0.326871	-0.326871	-0.326871
$X = 0.75$	-0.738724	-0.738724	-0.738724	-0.738724	-0.738653	-0.738653	-0.738653	-0.738653
$X = 1.00$	-1.223479	-1.223479	-1.223479	-1.223479	-1.223224	-1.223224	-1.223224	-1.223224

solution when N_T approaches 30, for all values of X and τ, unless on $\tau = 0.01$, mainly at positions closer to $X = 0$. It is observed that the values presented in this work are very close to those presented by Matt (2013). It is important to note that the convergence of this case in relation to the free vibration case is very similar, with no abrupt changes in values

from the beginning of the beam to the tip. This change is only not seen at the beginning of the beam in the first temporal instants, which have little relevance in practical terms.

PHYSICAL ANALYSIS

In this section, implementation results of all the terms considered in the modeling exposed in this work will be presented. Focus will be given to the influence of beam internal damping (λ), external damping (η), and tip mass characteristics (α, β, and ε) for free and forced vibration. For all cases, consider the same values proposed by Matt (2013), that is, an aluminum cantilever beam with Young's modulus E = 69 GPa and specific mass ρ = 2700 kg m^{-3}. The length of the beam is L = 1 m and it has a circular section with diameter D = 10 mm. The mass per unit length is μ = 0.212 kg m^{-1} and the first circular natural frequency without a tip mass is Ω = 44.442 rad s^{-1}. Consider as "damped" or "undamped" the presence or absence of internal damping, once in all cases the external damping is presented. It is worth mentioning that this configuration under analysis is not purely an abstraction with no practical application. This solution can represent the vibration of long beams, with a large mass at their tip, or small ones, with a tip mass proportional to the beam mass. The choice of analysis system proposed by this work, previously used by Matt (2013), is just one of the many possible real engineering situations this solution is able to represent.

Influence of Internal Damping on Free and Forced Vibration

In this section, the influence of the internal damping of the beam material is analyzed. For that, four cases will be studied, based on tip mass characteristics, damping values and excitation type. The parameter values of all cases studied in that section are presented on Tab. 4, where $\nu = 0.128191$.

Table 4 – Parameter values for free and forced vibration analysis, considering damped and undamped system.

System/Parameter	α	β	ε	η	λ	$F_0(\tau)$	$V_0(X)$
Free Damped	10	0.5	0.1	0.05	0.05	0	$0.225\sin(\pi X)$
Free Undamped	10	0.5	0.1	0.05	0	0	$0.225\sin(\pi X)$
Forced Damped	20	1.0	0.2	0.05	0.05	$0.5\sin(\nu\tau)$	0
Forced Undamped	20	1.0	0.2	0.05	0	$0.5\sin(\nu\tau)$	0

For free vibration dynamics, consider $N_T = 50$ a sufficient value for the series to converge to at least six decimal places, as exposed on Tab. 2. The solution for damped and undamped beams in free vibration can be seen in Fig. 2 (left-side hand). For forced vibration, $N_T = 60$ was considered a sufficient value for the series to converge to at least six decimal places, as exposed on Tab. 3. The solution can be seen in Fig. 2 (right-hand side).

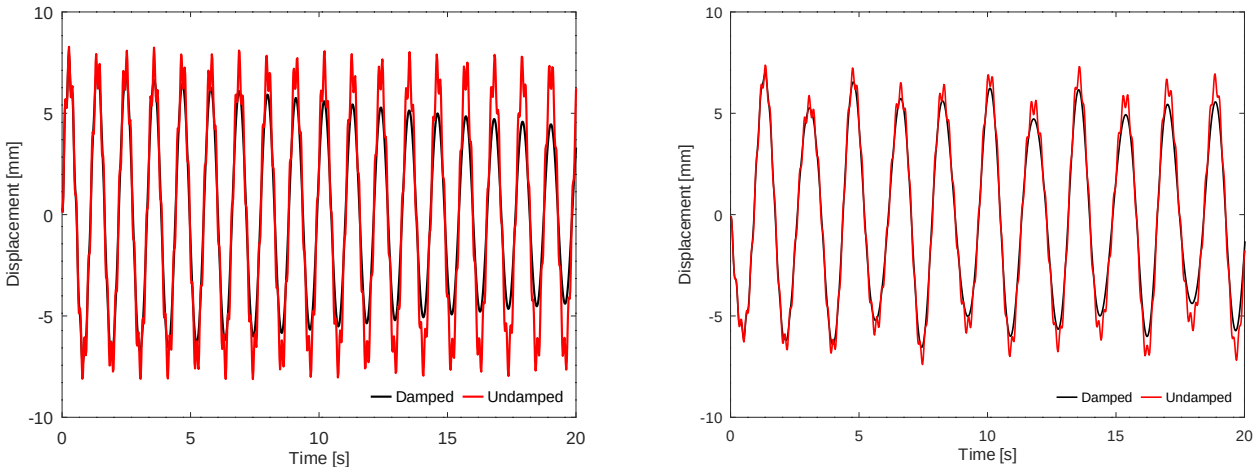

Figure 2 – Deflection of the cantilever beam with tip mass at x = L on free (left-hand side) and forced (right-hand side) vibration.

From Fig. 2, based on free vibration system, it can be seen that, unlike a free vibration with no tip mass, the tip mass creates perturbations in the nodes and anti-nodes of the graph. Without the tip mass, these nodes and anti-nodes would be continuous and without irregularities. Furthermore, it can be seen that the amplitude at t = 0 s and t = 20 s in free vibration without internal damping is practically equal. In the damped case, there is a very prominent reduction of this amplitude. Corroborating this point, it can be seen that the amplitude in the first moments reaches the mark of 9 mm and, when the damped system arrives in 20 s, this amplitude is less than 5 mm. Finally, it is possible to observe that the irregularities in the vibration nodes and anti-nodes without internal damping are quickly dispersed in damped vibration,

reducing them to almost zero in approximately 5 s. In the first seconds of the transient, it is still possible to observe these irregularities in damped vibration, which is very similar to the undamped one. From the second node, there is a sudden reduction in amplitude and irregular behavior of the damped vibration, rapidly tending to a regular oscillation. Thus, the internal damping tends to dampen the noise caused by the tip mass in the nodes and anti-nodes in free vibration. Based on the curve referring to the forced vibration, internal damping has a relevant impact on the regularization of the nodes and anti-nodes, as mentioned in free vibration. From the first oscillation, the non-compliance of the damped solution with the irregularities of the undamped solution is already noticeable. In terms of amplitude, there is a subtle but noticeable change in all nodes and anti-nodes since the beginning of the vibration. It is observed that, with internal damping, the beam vibrates as if there were no mass at the tip, smoothing the oscillatory behavior.

From an inverse problem perspective for identifying physical parameters in real applications, this information is quite relevant. As the internal damping has a greater impact on free vibration, it is possible to assume that it will have greater sensitivity in this type of vibration. Thus, it is likely that experimental data that contain the forced part of the vibration and the free part (considering an experiment with shaker on and abruptly off) are better used for this type of survey.

Tip Mass Influence on Free and Forced Vibration on Damped and Undamped Systems

In this section, the influence of the tip mass on free and forced vibration, considering damped and undamped systems is analyzed. The parameter values of all cases studied in that section are presented on Tab. 5, where $\nu = 0.128191$. In this study is considered two types of system: the one with a "big tip mass" (BTM) and the one with a "small tip mass" (STM). The term BTM and STM are relative to an increase and decrease of tip mass influence consider as reference the values of α, β and ε presented in the results on "Computational Verification" section. For free and forced vibration, consider $N_T = 50$ and $N_T = 60$, respectively. On Figure 3 and 4 are presented the dynamic of the BTM and STM systems on free and forced vibration, respectively.

Table 5 – Parameter values for free and forced vibration analysis, considering damped and undamped systems with BTM and STM.

System/Parameter	α	β	ε	η	λ	$F_0(\tau)$	$H_0(\tau)$	$V_0(X)$
Free Damped BTM	20	1	0.2	0.05	0.05	0	0	$0.225\sin(\pi X)$
Free Damped STM	5	0.25	0.05	0.05	0.05	0	0	$0.225\sin(\pi X)$
Free Undamped BTM	20	1	0.2	0.05	0	0	0	$0.225\sin(\pi X)$
Free Undamped STM	5	0.25	0.05	0.05	0	0	0	$0.225\sin(\pi X)$
Forced Damped BTM	20	1	0.2	0.05	0.05	$0.5\sin(\nu\tau)$	$0.5\sin(\nu\tau)$	0
Forced Damped STM	5	0.25	0.05	0.05	0.05	$0.5\sin(\nu\tau)$	$0.5\sin(\nu\tau)$	0
Forced Undamped BTM	20	1	0.2	0.05	0	$0.5\sin(\nu\tau)$	$0.5\sin(\nu\tau)$	0
Forced Undamped STM	5	0.25	0.05	0.05	0	$0.5\sin(\nu\tau)$	$0.5\sin(\nu\tau)$	0

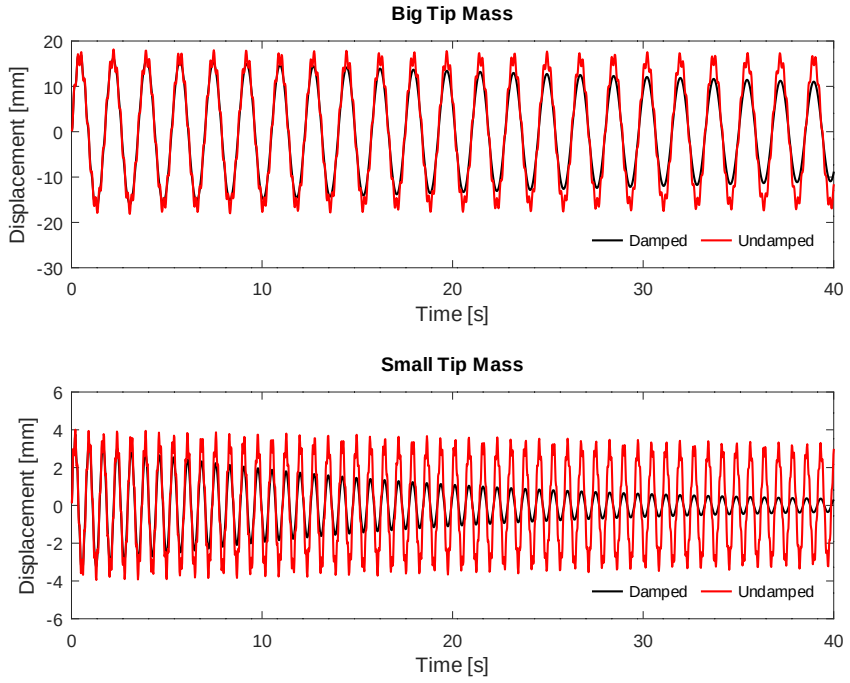

Figure 3 – Deflection on free vibration of the cantilever beam with tip mass at x = L considering damped and undamped system, considering two different tip mass characteristics.

It is observed that the internal damping strongly modifies the amplitude variation in free vibration compared to the impact of the external damping. It's worth pointing out that, in both cases, the regulation of nodes and anti-nodes irregularities is performed, regardless of the size of the mass at the tip. Finally, given the tip mass inertia present in the system where it is greater, there is great difficulty in damping the system. In this way, larger tip masses can be used to keep a more damped system in motion.

On Figure 4 is presented the forced vibration system deflection, considering BTM and STM. On the right of vibration displacement is shown the absolute difference between damped and undamped response for better visualization of results. It is worth pointing out that the scale of forced vibration with BTM is twice the scale of forced vibration with STM.

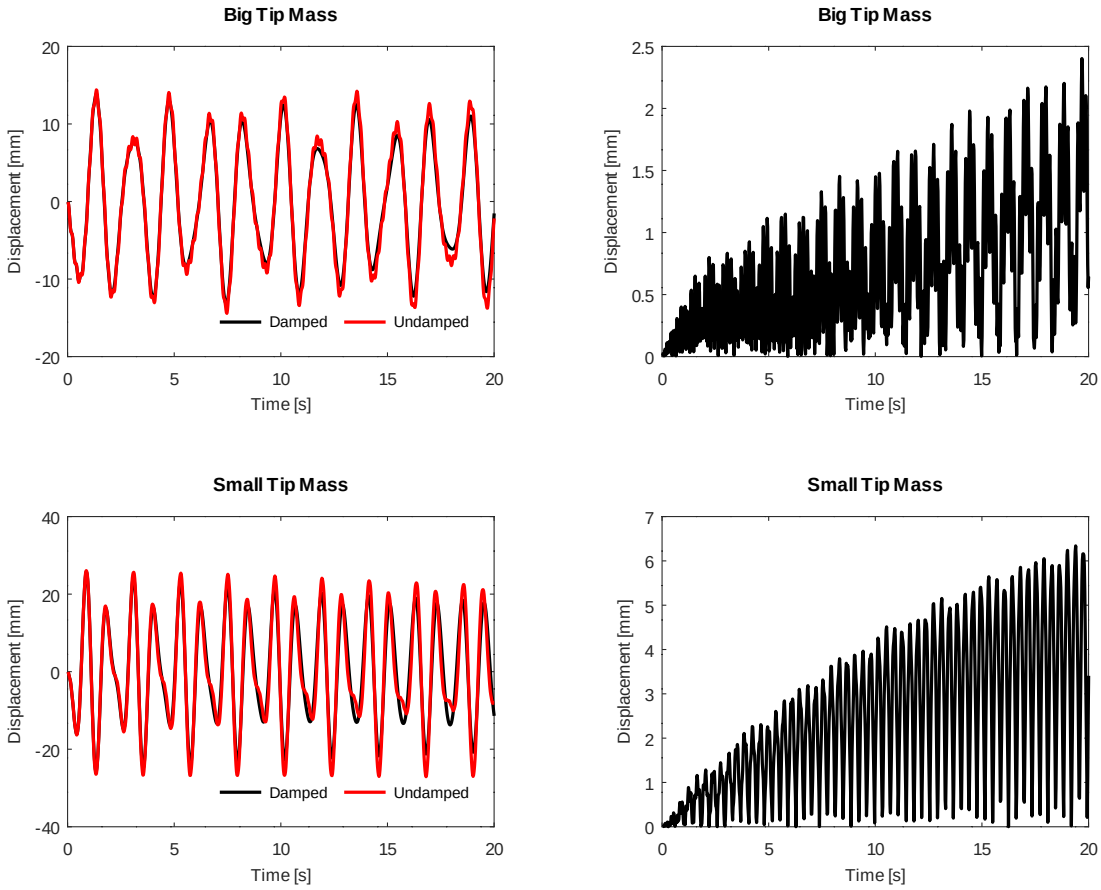

Figure 4 – Deflection on forced vibration of the cantilever beam with tip mass at x = L considering damped and undamped system, considering two different tip mass characteristics.

In this situation, internal damping results in two very different behaviors. In the case where the tip mass is more robust, little change is noticeable. In this case, there is only a regularization of the nodes and anti-nodes, maintaining the dynamics of the undamped system. At the other hand, the internal damping modifies substantially the nodes and anti-nodes amplitude on the system with STM. It's possible to see that, next to 20 s, the amplitude difference on the anti-node between the damped and undamped system is more than 6 mm, a relative difference gratter than 22%. So, it can be seen that the modification of the tip mass modified the influence of the internal damping in a much more intense way than the external damping, for example. Thus, it is clear the need to survey this property depending on the system under analysis.

CONCLUSIONS

In this work, an analytical solution via the Generalized Integral Transform Technique (GITT), based on the implementation of an implicit filter and eigenfunction expansion, was presented for a vibrational problem of a cantilever viscoelastic Euler Bernoulli beam, considering an eccentric tip mass, oscillating base, external damping and an external excitation as a spatial and temporal function throughout the beam. By physical analysis, it can be seen that the influence of internal damping can be much higher than the influence of external damping, depending on the characteristics of the system. As an elastic material is theoretically an abstraction, that is, all material has some internal damping, a careful analysis of the influence of this structural behavior of the material on the mechanical vibration of systems can be carried out from the modeling presented in this work, both for forced and free vibration. The solution of this model can be further refined to represent the influence of other physics and even more complex problems, such as fractional internal damping, fractional external damping, axial forces, and vertical eccentricity of the tip mass center of gravity.

ACKNOWLEDGMENTS

The authors would like to thank Dr. Erb F. Lins (UFRPE) for his valuable contributions on computational programming and Dr. Joshua J. Goings (Google Quantum AI) for elucidating biorthogonalization issues from his writings available on his website. This study was financed in part by the Coordenação de Aperfeiçoamento de Pessoal de Nível Superior – Brasil (CAPES) – Finance Code 001.

REFERENCES

Abdulraheem, K. F., Al-Kindi, G., 2018, "Wind Turbine Blade Fault Detection Using Wavelet Power Spectrum and Experimental Modal Analysis", International Journal of Renewable Energy Research (IJRER), Vol. 8, No. 4, pp. 2167 - 2179.

Adhikari, S., Bhattacharya, S., 2021, "A general frequency adaptive framework for damped response analysis of wind turbines", Soil Dynamics and Earthquake Engineering, Vol. 143, pp. 106605.

Almeida, A. P., Naveira-Cotta, C. P., Cotta, R. M., 2020, "Transient three-dimensional heat conduction in heterogeneous media: Integral transforms and single domain formulation", International Communications in Heat and Mass Transfer, Vol. 117, pp. 104792.

Carvalho, I. S., Cotta, R. M., Naveira-Cotta, C. P., Tiwari, M. K., 2021, "Hybrid integral transform analysis of supercooled droplets solidification", Proceedings of the Royal Society A, Vol. 477, No. 2248, pp. 20200874.

Chen, W. H., Lu, Z. R., Lin, W., Chen, S. H., Ni, Y. Q., Xia, Y., Liao, W. Y., 2011, "Theoretical and experimental modal analysis of the Guangzhou New TV Tower", Engineering Structures, Vol. 33, No. 12, pp. 3628 - 3646.

Dehand, M., Jahani, K., Sadeghi, M., Afagh, F. F., 2022, "Studying effects of joint characteristics on the performance of a cantilever beam shaped piezoelectric energy harvester through joint identification", Journal of Intelligent Material Systems and Structures, Vol. 33, pp. 1588-1601.

Hijmissen, J. W., Van Horssen, W. T., 2008, "On the weakly damped vibrations of a vertical beam with a tip-mass", Journal of Sound and Vibration, Vol. 310, No. 3, pp. 740 - 754.

Matt, C. F. T., 2013, "Simulation of the transverse vibrations of a cantilever beam with an eccentric tip mass in the axial direction using integral transforms", Applied Mathematical Modelling, Vol. 37, No. 22, pp. 9338 - 9354.

Rahman, M., Ong, Z. C., Chong, W. T., Julai, S., Ng, X. W., 2019, "Wind turbine tower modeling and vibration control under different types of loads using ant colony optimized PID controller", Arabian Journal for Science and Engineering, Vol. 44, No. 2, pp. 707 - 720.

Rama Bhat, B., Wagner, H., 1976, "Natural frequencies of a uniform cantilever with a tip mass slender in the axial direction", Journal of Sound Vibration, Vol. 45, No. 2, pp. 304 - 307.

Silva, G. R.. Knupp, D. C., Naveira-Cotta, C. P., Cotta, R. M., Silva Neto, A. J., 2020, "Estimation of slip flow parameters in microscale conjugated heat transfer problems", Journal of the Brazilian Society of Mechanical Sciences and Engineering, Vol. 42, No. 5, pp. 1 - 16.

Wahrhaftig, A. M., Silva, M. A., Brasil, R. M. L. R. F., 2019, "Analytical determination of the vibration frequencies and buckling loads of slender reinforced concrete towers", Latin American Journal of Solids and Structures, Vol. 16.

RESPONSIBILITY NOTICE

The authors are the only responsible for the printed material included in this paper.